INSTITUTE OF PHYSICS PUBLISHING JOURNAL OF PHYSICS D: APPLIED PHYSICS

J. Phys. D: Appl. Phys. **36** (2003) 1620–1628 PII: S0022-3727(03)55762-X

Fracture induced electromagnetic radiation

V Frid[1], A Rabinovitch[2] and D Bahat[1]

[1] Geological and Environmental Sciences Department, The Deichmann Rock Mechanics Laboratory of the Negev, Ben Gurion University of the Negev, Beer Sheva, Israel
[2] Physics Department, The Deichmann Rock Mechanics Laboratory of the Negev, Ben Gurion University of the Negev, Beer Sheva, Israel

E-mail: vfrid@bgumail.bgu.ac.il, avinoam@bgumail.bgu.ac.il and bahat@bgumail.bgu.ac.il

Received 8 November 2002, in final form 8 April 2003
Published 18 June 2003
Online at stacks.iop.org/JPhysD/36/1620

Abstract
In our laboratory, we combine accurate electromagnetic radiation (EMR) measurements during fracture of rocks (carbonate and igneous) and transparent materials (glass, PMMA and glass ceramics) with careful fractographic methods. A critical analysis of experimental observations, accumulated here during the last decade together with supporting material from the works of other authors are used in this study to demonstrate the failure of all current models to explain the properties of EMR arising from fracture. The basic elements of a new model are proposed. These are (a) the EMR amplitude increases as long as the crack continues to grow, since new atomic bonds are severed and their contribution is added to the EMR. As a result, the atoms on both sides of the bonds are moved to 'non-equilibrium' positions relative to their steady state ones and begin to oscillate collectively in a manner similar to Debye model bulk oscillations—'surface vibrational optical waves'; (b) when the crack halts, the waves and the EMR pulse amplitude decay by relaxation. These basic elements are already enough to describe the characteristics of the experimentally obtained isolated individual EMR pulses. These characteristics include the shape of the EMR pulse envelope, and the frequency, time duration and rise–fall time of the pulse.

1. Introduction

The fracture of material induces the emission of electrons and positive ions, neutral atoms and molecules, visible photons and radio waves (Urusovskaja 1969, Langford and Dickinson 1987, Enomoto and Hashimoto 1990). This paper considers only electromagnetic radiation in the frequency range 10 kHz–50 MHz (denoted here by EMR). EMR from materials fractured under compression was first observed by Stepanov in 1933 for samples of sylvine (KCl) (Urusovskaja 1969). This investigation was followed by numerous others, which measured EMR from a very wide range of piezo and non-piezoelectric, crystalline and amorphous, metallic and non-metallic materials and rocks under different stress loadings (e.g. Nitsan 1977, Warwick *et al* 1982, Khatiashvili 1984, Ogawa *et al* 1985, Cress *et al* 1987, Yamada *et al* 1989, O'Keefe and Thiel 1995, Ueda and Al-Damegh 1999, Yoshida 2001).

Following these investigations, the interest in fracture-emitted EMR shifted from the basic nature of the phenomenon to a more applied nature connected to problems of earthquake prognosis (Warwick *et al* 1982, King 1983, Khatiashvili 1984, Hayakawa *et al* 1993, Ueda and Al-Damegh 1999, Yoshida 2001), the forecast of rock failure in underground mines (Khatiashvili 1984, Frid 1997, 1998, 2000, 2001, Vozoff and Frid 2001) and the study of explosions (Sakai *et al* 1992, Tomizawa *et al* 1994, Tomizawa and Yamada 1995, Rabinovitch *et al* 2002a).

Previous attempts to explain the origin of EMR from fracture were, unfortunately, unable to explain all the features of the detected radiation (King 1983, Rabinovitch *et al* 1995, 1996, 1998, Freund 2000, 2002). This paper presents experimental investigations conducted in our laboratory and other supporting evidence that demonstrate the actual failure of the existing theories. Furthermore, we formulate the foundations of a more sophisticated model for the origin of

EMR from fracture. This model is based both on our previous results as well as some new ones.

2. Previous models

2.1. Dislocations and charged electrons

Misra (1977) and Misra and Ghosh (1980) suggested that 'during non-uniform distribution of dislocations, which occur at the transition stages of elastic–plastic deformation under tension, namely, yield point, end of Luders' strain, crack propagation and fracture, mobile dislocations arrange themselves into some configuration, that is mechanically stable'. If, at the halting position of a dislocation, its energy is reduced, the dislocation can become self-trapped. 'Conduction electrons (CEs), associated with such a dislocation, would be stopped and trapped relative to the positive ions'. This CE 'braking' process would be similar to a 'Bremsstrahlung' mechanism and would result in the emission of EMR. Misra (1977) further assumed that: 'during each transition stage (like a yield point and/or fracturing) there must be a re-adjustment of the CE distribution within the microscopic system, and the latter creates an oscillating Hertzian dipole. Thus, the EMR must appear only at transition deformation stages'.

As an opposing analysis Molotskii (1980) pointed out that in the adjustment of the CEs to the slowly moving dislocations, their acquired energy would be of the order of 10^{-11} eV per mean free path, so that the maximum frequency of emitted EMR would be of the order of 10^3 Hz, i.e. significantly lower than the values predicted and measured by Misra; therefore, the acceleration of CEs by moving dislocations could not be the cause of the EMR from metals, and Molotskii suggested that the EMR was rather due to the increase of the total dislocation length and velocity, which occurred at transient deformation stages. Since these dislocations acted as electric dipoles, this mechanism would lead to an accelerated rise in the dipole moment of the material with the accompanying emission of EMR.

Both explanations, however, relating EMR to dislocation phenomena seem questionable. As is well known the motion of dislocations can be totally neglected in the cracking of brittle materials, and this mechanism therefore cannot explain EMR from glass and other brittle materials (e.g. most geological materials). A typical EMR pulse from the failure of a glass cylinder under uniaxial compression is shown in figure 1. The shape of EMR signals remains unchanged for different brittle materials such as glass, glass ceramics, granite, rhyolite, limestone and chalk (Rabinovitch *et al* 1995, 1996, 1998–2000, Frid *et al* 1999, 2000, Bahat *et al* 2001, 2002), and is even unaltered under different types of loading (compression, drilling and blasting (Goldbaum *et al* 2001, Rabinovitch *et al* 2002b), and mining (Vozoff and Frid 2001).

This basic weakness of the 'dislocation movement hypothesis' was also pointed out by Jagasivamani and Iyer (1988), who showed experimentally that the EMR amplitude even increased with the brittleness of the investigated metals. Indeed, this latter result is in the context of our measurements (Frid *et al* 1999), which also showed that the EMR activity increased with the brittleness of materials and decreased in the case of transition from brittle to ductile behaviour (the

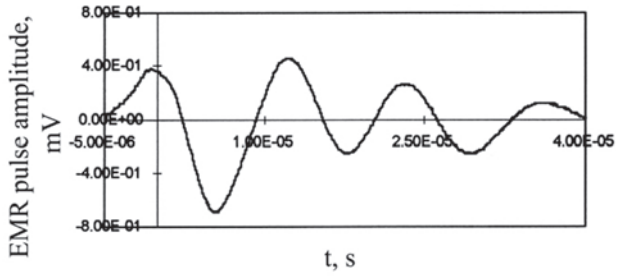

Figure 1. A typical EMR pulse observed during glass cylinder failure under uniaxial compression.

beginning of the brittle–ductile transition was confirmed by the large angle ($41^\circ \pm 1^\circ$) produced between the axial axis and the failure plane and by the insignificant increase of the shear strength.

2.2. Discharge

Finkel *et al* (1975) demonstrated that the splitting of alkali halide crystals creates a mosaic of positive and negative charges, which appear on both sides of the fracture as it is formed. Since such charge separation can create an electrostatic field of the order of 10^7 V cm^{-1}, an electric discharge may occur, which was suggested as the origin of EMR. However, already Miroshnichenko and Kuksenko (1980) and Khatiashvili (1984) noted that the spectrum of the discharge radiation is known to be of the 'white noise' type and to be independent of the mechanical properties of the materials; yet, the observed EMR behaves in an entirely different manner (Miroshnichenko and Kuksenko 1980, Rabinovitch *et al* 1998, 1999, Frid *et al* 2000). Our results show that the EMR appears as individual pulses or as clusters of pulses caused by the different (individual or group) fractures (Rabinovitch *et al* 1999, 2000, 2002a, Frid *et al* 2000). The properties of a pulse are influenced by the fracture dimensions (see below) (Rabinovitch et al 1998, 1999, 2000, Frid *et al* 2000) and are dependent on the elastic properties of the materials (Khatiashvili 1984, Frid *et al* 1999). Moreover, the high resolution of our experimental system (Rabinovitch *et al* 1998) facilitates the analysis of the exact shapes of the EMR pulses (figures 1 and 2). These, definitely, do not behave as 'white noise' but rather exhibit a very distinct character (see later). These results are similar to those observed by Miroshnichenko and Kuksenko (1980) and Khatiashvili (1984). Note, in particular, that the EMR spectrum (figure 2) is highly localized around a single frequency.

2.3. Movement of fracture tips

EMR is observed (Gershenzon *et al* 1986) during the propagation of cracks induced by cleavage of LiF crystals with a knife. The developing crack (tip) propagates in the direction of indentation. According to the author's assumption, negative electrical charge moves with the crack tip while positive charge is assumed to accumulate at the region of the indenter–material contact. Dipole radiation should occur from these opposite charges, separated by the length of the crack, by the deceleration of the crack. Based on these assumptions, the power of the emanating EMR was calculated

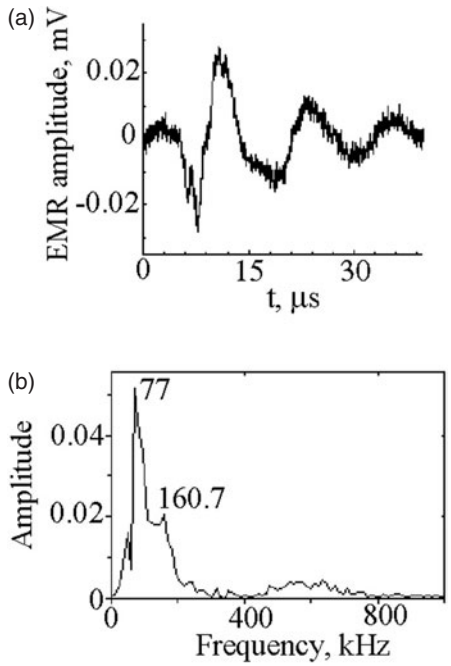

Figure 2. An example of EMR signal excited by fracture of granite in compression (*a*) and its spectrum (*b*).

by Gershenzon *et al* (1986), who further assumed that the charging mechanism arose from moving charged dislocations.

As already pointed out, however, charge transfer by dislocations cannot constitute a general explanation of the origin of EMR, and even for a dielectric like LiF the 'movement of fracture tips' explanation is questionable (Tetelman and McEvly 1967), since the velocity of dislocations in alkali halide crystals is smaller than the velocity of the crack, implying that charged dislocations could not be the reason for crack tip charging.

An even stronger adverse argument is that there is no clear reason for any 'symmetry breaking', i.e. there is no known mechanism which would select tip (side) 'A', say, to become negative while the other tip (side) to become positive and not vice versa. In particular, for the case discussed by Gershenson *et al* (1986) it is not clear why the crack tip should accumulate negative but not positive charge.

2.4. Movements of fracture sides (the 'capacitor' model)

In order to determine whether movements of the crack sides during cracking could cause EMR with the appropriate characteristics, Miroshnichencko and Kuksenko (1980) used the acoustic wave emitted by a fracturing material to drive the plates of a specially built auxillary charged capacitor. The EMR from the capacitor was monitored by an antenna. Since the measured signal 'shapes' were comparable to those obtained by the 'directly' observed EMR, they concluded that the latter was caused by similar movements of the charged sides of the crack.

A decade later, O'Keefe and Thiel (1995) suggested another version of a capacitor model (for EMR from the cracking of compressed ice), in which a charged parallel plate capacitor is created whose plates (crack sides) are being drawn apart. After an initial charge is formed on the crack surfaces, further separation should result in a decrease of capacitance and a resulting increase in the voltage across the crack. A space/time analysis of the emanating radiation can be carried out using the diffusion equation for the electric field in the crack. Although by the use of this method it was possible to simulate the time decay of the EMR, no oscillatory behaviour was predicted. O'Keefe and Thiel (1995) also considered the many routes by which the net charge could be created: i.e. pre-polarization of the material or applied physical gradients due to piezoelectricity or pseudo-piezoelectricity, temperature, deformation, impurity concentration gradient effects, etc Petrenko (1993) claimed that the electrification of crack sides could be caused by the surrounding non-homogeneous elastic strains, and Ogawa *et al* (1985) assumed that crack sides electrification was due to piezoelectrification and contact (or separating) electrification. These latter studies argued that if two rocks of different work-functions were in contact, electrons would move across the potential barrier at the contact surface, producing a potential difference between the rocks, and an electric double layer would appear across the contact plane. On the other hand, when a multimineral rock sample such as granite was broken into two pieces, a different process of charge movement would occur: electrons should move back from the rock of lower contact potential to the rock of higher potential.

However, the whole 'capacitor' scenario is rather questionable for the following reasons.

(a) In this model the EMR is assumed to be caused by an accelerated dipole created by charged crack sides. This assumption implies that the EMR can arise only from tensile cracks and not from shear ones. Our measurements of chalk under uniaxail and triaxial compression (Frid *et al* 2000) show a different result. We selected chalk for our study due to its micro-texture and low strength leading to a relatively small number of fragments at failure, which can be analysed fractographically (Bahat 1991, Bahat *et al* 2001). Our measurement indeed showed a clear fractographic distinction between fractures originating from tension and those originating from shear.

The total EMR amplitude (measured above the sample's elastic limit) (figure 3) was fitted (squared regression coefficient $R^2 = 0.86$) to the linear equation:

$$E = -33.39 + 0.006\,55S_t + 0.005\,96S_s$$

where E is the total compensated EMR pulse amplitude ($V\,m^{-1}$), and S_t and S_s are the total areas (mm^2) of the tensile and shear cracks, respectively. The two coefficients multiplying S_t and S_s are the same to within $\pm 5\%$, which is of the order of the error in our area measurements. This result demonstrates that the EMR amplitude is independent of crack mode (tensile or shear), and is related only to the entire area of the crack (Frid *et al* 2000).

(b) The pulse shapes (figures 1 and 2) provide an additional argument. These shapes agree with the measurements of Miroshnishencko and Kuksenko (1980) but not with those of O'Keefe *et al* (1995), so that O'Keefe's model cannot explain both our results and those of Miroshnishencko and

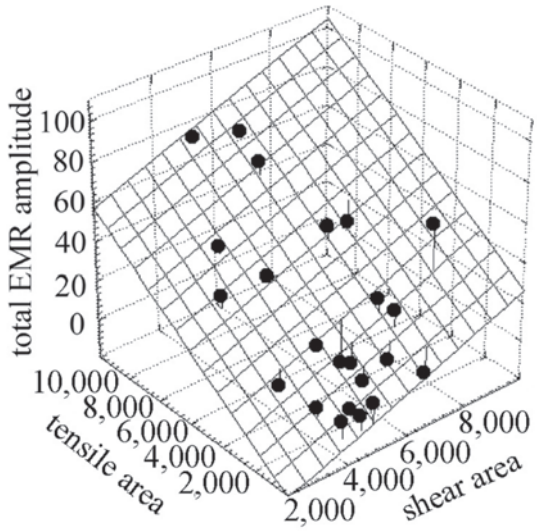

Figure 3. A three-dimensional experimental graph of total compensated EMR pulse amplitudes (V m^{-1}) vs total tensile and shear crack areas (mm^2) of all investigated samples and its linear fit (see text).

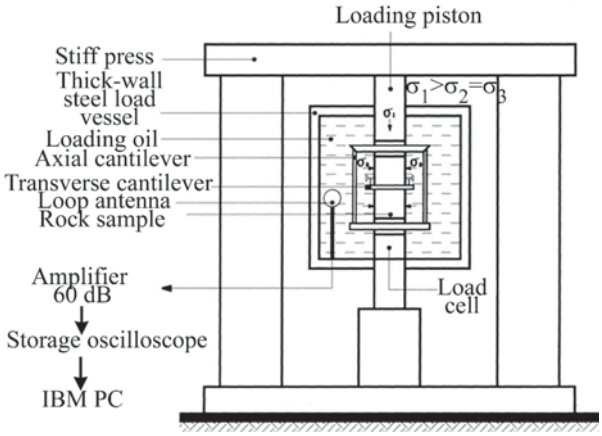

Figure 4. Schematic diagram of the experimental arrangement.

Kuksenko (1980). At any rate, the capacitor model implies a correspondence between EMR and the appearance of acoustic emission (AE) signals. However, our own measurements and those of Yamada *et al* (1989) show that although there are failure events for which AE and EMR signals are measured together (e.g. Rabinovitch *et al* 1995), there do exist events for which AE is detected whereas EMR is absent and events for which EMR is observed and AE is completely missing. These results therefore disagree with the capacitor model. Note that the latter discord between the appearance of AE and EMR signals is probably due to the difference in mechanisms leading to the two types of radiation, and is not yet completely understood.

In addition, the general 'no symmetry breaking' argument mentioned above evidently applies here as well.

(c) Even under the assumptions that the two crack sides could be charged in a charge mosaic manner (Finkel *et al* 1975), thus retaining an overall charge neutrality, and that the EMR was induced by the dipoles consisting of pairs of oppositely charged mosaic 'elements' on the two crack sides, the EMR induced by the moving crack would be expected to be very weak due to the cancellation of the radiation originating from mutually oscillating oppositely charged dipoles (random distribution of the mosaic elements).

In summary, all the hitherto suggested models for the origin of EMR fail to stand the tests of experiment and/or self-consistency. In the following, we outline the basis of a more favourable model.

3. EMR pulse shape parameters

3.1. Experimental arrangement

A triaxial load frame (TerraTek stiff press model FX-S-33090; axial pressure up to 450 MPa; confining pressure up to 70 MPa; stiffness $5 \times 109\,\mathrm{N\,m^{-1}}$) was used for the measurement (figure 4). It is combined with a closed-loop servocontrol (linearity 0.05%), which is used to maintain a constant axial piston rate of displacement. The load was measured with a sensitive load cell (LC-222M, maximum capacity 220 kN, linearity 0.5% full scale). The confining pressure was continually controlled by a clock-type sensor to preserve its preset value through volumetric changes of the sample during the loading process. The cantilever set (consisting of axial and lateral detectors; strain range about 10%; linearity 1% full scale) enabled us to measure sample strains in three orthogonal directions, parallel to the three principal stresses.

A magnetic one-loop antenna (EHFP-30 Near Field Probe set, Electro-Metrics Penril Corporation) 3 cm in diameter was used for the detection of the EMR. It is wound within a balanced Faraday shield, so that its response to external electric fields is vanishingly small. A low-noise, micro-signal amplifier (Mitek Corporation Ltd, frequency range 10 kHz–500 MHz, gain 60 ± 0.5 dB, noise level 1.4 ± 0.1 dB across the entire frequency band) and a Tecktronix TDS 420 digital storage oscilloscope connected by way of a General Purpose Interface bus to an IBM PC, completed the detection equipment.

The entire system 'antenna–amplifier–storage oscilloscope', was carefully adjusted to an input–output impedance of 50 Ω.

The antenna was placed 2 cm away from the centre of the loaded samples with its normal pointing perpendicular to the cylinder axis. The EMR was monitored in the frequency band from 10 kHz up to 50 MHz with an overall sensitivity of up to 1 μV.

3.2. Pulse parametrization

A semi-empirical analysis of the EMR signals was carried out. The signals's general shape including its envelope, frequency and duration can be obtained by our basic (see later) theory, while the parameters themselves were derived by least squares fitting of the experimental results. The signal shape is given

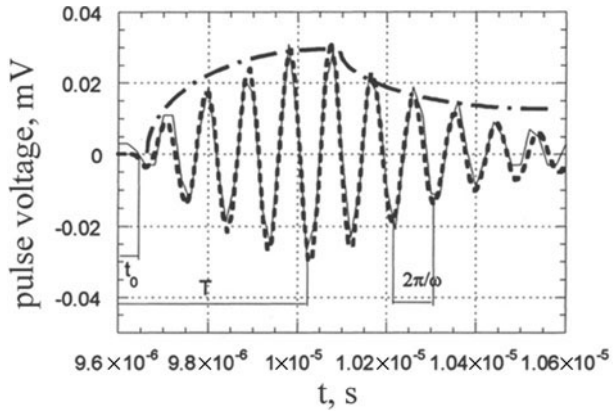

Figure 5. An experimental EMR pulse (——), its numerical fit (- - - -) and envelope (— · —).

by (Rabinovitch *et al* 1998)

$$A = \begin{cases} A_0 \sin(\omega(t-t_0))\left(1-\exp\left(-\dfrac{t-t_0}{\tau}\right)\right) \\ \quad t < T \\ A_0 \sin(\omega(t-t_0))\exp\left(-\dfrac{t-T}{\tau}\right) \\ \quad \times\left(1-\exp\left(-\dfrac{T-t_0}{\tau}\right)\right) \qquad t \geqslant T \end{cases} \tag{1}$$

where t is the time, t_0 is the time from the origin up to the beginning of the pulse and T is the time from the origin up to the maximum of the EMR pulse envelope. Thus, $T' = T - t_0$ is the time interval to reach pulse maximum, τ is the pulse rise time and fall time (see later), which are identical within experimental uncertainty (Rabinovitch *et al* 2003), ω is the frequency and A_0 is the pulse peak amplitude. A representative example is shown in figure 5. The parameters A_0, T', ω and τ were derived by a least squares fit (Rabinovitch *et al* 1998).

Three basic elements of a physical model, which would result in such a simple relationship are the following.

(a) Time dependence of the envelope of the EMR pulse amplitude $A(t)$. We have already shown (Rabinovitch *et al* 1998) that 'A' increases as long as the crack continues to grow, since new atomic bonds are severed and their contribution is added to the EMR. When the crack halts, the pulse amplitude starts to decay. The time from the start of the pulse up to its maximum, T', should be proportional to the number of severed atomic bonds and thus to the crack length l (the crack velocity $v_{\rm cr}$ is almost constant).

$$T' \sim \frac{l}{v_{\rm cr}} \tag{2}$$

In the time increment, $\mathrm{d}t$, the amplitude of the envelope of the EMR 'A' decreases by dissipation to $A(t)(1-\mathrm{d}t/\tau)$, but it is 'replenished' by a term proportional to the number of severed bonds, $\alpha\,\mathrm{d}x$, where '$\mathrm{d}x$' is the length increment of the crack in the interval '$\mathrm{d}t$' ($\mathrm{d}x = v_{\rm cr}\,\mathrm{d}t$) and α is a coefficient relating the antenna output to '$\mathrm{d}x$'. α is assumed to be proportional to the width of the crack 'b' (the following calculations assume a constant crack width), to the number of bonds per unit area, to the emittence of a bond, to the solid angle of the crack seen by the antenna and to the latter's conversion factor. It follows that

$$\frac{\partial A}{\partial t} = -\frac{A}{\tau} + \alpha v_{\rm cr} \tag{3}$$

Hence,

$$A = \alpha v_{\rm cr}\tau(1-\mathrm{e}^{-t/\tau}) \qquad t_0 \leqslant t < T \tag{4}$$

For $t > T$, the crack stops growing and the amplitude thereafter diminishes, resulting in

$$A = A(T)\mathrm{e}^{-t/\tau} \qquad t \geqslant T \tag{5}$$

In figure 5 the shape of the envelope (equations (4) and (5)) is shown by a dash-dotted line.

(b) Regarding, the oscillatory parts of equation (1) we assume that these EMR waves are created by charge oscillations on both sides of the propagating crack (see figure 6). Consider the line of bonds located at the front (tip) of the propagating crack (figure 6(*a*)). These bonds break when the front moves to the next line. Following this break, the atoms on both sides of the bonds are moved to 'non equilibrium' positions in relation to their steady state ones and will perform oscillations around them. If each atom (ion) vibrated individually, the situation would resemble the Einstein model of lattice vibrations and the frequency of these oscillations would approach 10^{15} Hz. Since, however, the lines of vibrating atoms move together and are also connected to atoms around them (in the forward direction and also to atoms on their side of the two surfaces newly created by the fracture) the ensuing vibrations are similar to those obtained for the bulk by the Debye model, having much lower frequencies. It is the oscillations stimulated by this process at the new surfaces, which give rise to the EMR, as follows. The positive charges on these surfaces move together in one direction away from the equilibrium plane (one crack side) while the negative charges move in unison in the other direction from the equilibrium plane (the same crack side), and vice versa, retaining an overall charge neutrality throughout. These surface oscillations, similar to Rayleigh waves, decay exponentially into the bulk (figures 6(*b*) and (*c*))—'surface vibrational optical waves (SVOW)' (e.g. Srivastava 1990), much like 'bulk optical (phonon) waves' (e.g. Kittel 1987) observed in vibrating crystals.

(c) It has been shown elsewhere (e.g. Srivastava 1990) that surface waves decay in time as a result of an interaction with bulk phonons. We, therefore (Rabinovitch *et al* 2003), consider τ to be the relaxation time of such a surface (Rayleigh-like) wave, which interacts with a bulk phonon, leading to the creation of another bulk phonon (a three-phonon process), and use equation (13) of King and Sheard (1970) to characterize the process. The rate of occurrence of the process per unit time, is given by the golden rule formula (Schiff 1986):

$$P_{\rm i}^{\rm f} = \frac{2\pi}{\hbar}|\langle f|H_3|i\rangle|^2\delta(E_{\rm f}-E_{\rm i})$$

where the initial and the final states are

$$|i\rangle = |n_{\rm R}, n_{\rm b1}, n_{\rm b2}\rangle, \qquad |f\rangle = |n_{\rm R}-1, n_{\rm b1}-1, n_{\rm b2}+1\rangle$$

H_3 is the time-dependent anharmonic part of the crystal Hamiltonian, $n_{\rm R}$, $n_{\rm b1}$ and $n_{\rm b2}$ are the numbers of surface phonons, initial and final bulk phonons, respectively. $E_{\rm i}$ and $E_{\rm f}$ are the initial and the final energies of the three-phonon system, so that $E_{\rm f} - E_{\rm i} = \hbar(\omega_{\rm b2} - \omega_{\rm R} - \omega_{\rm b1})$, where the ω

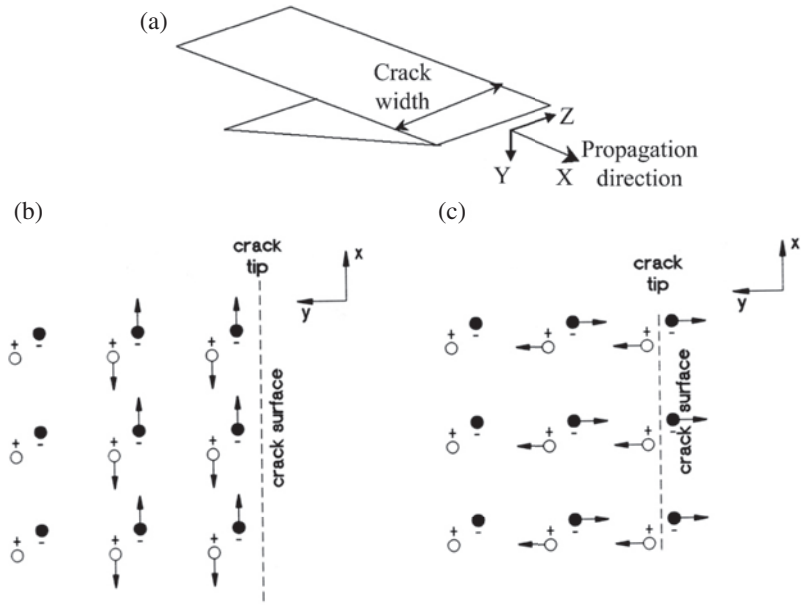

Figure 6. (*a*) A schematic picture of crack propagation; (*b*) and (*c*) schematic 'optical surface wave' at crack surface (a similar wave propagates on the other surface) at a specific time. Crack surface is in the xz plane and the crack moves in the x-direction. Note that charge separation can either be longitudinal (*b*) or transverse (*c*) with respect to the surface, with appropriate EMR polarizations. Note also the exponential decay of the wave into the material. Charge separation is oscillatory so that at a later time the dipole directions are reversed.

denote the related frequencies. The relaxation time τ, which we identify with the rise and fall time of the EMR pulse, is obtained from the golden rule formula ($1/\tau$ being proportional to the transition probability) using the explicit expression for H_3 (equation (6.47) in Srivastava 1990), and the displacement field due to the surface modes written in second quantized notation. Integrating over the states of the initial and final bulk phonons b_1 and b_2, one obtains (equation (8.36), Srivastava 1990)

$$\frac{1}{\tau_{\mathrm{R}}} \propto \frac{\omega_{\mathrm{R}} T^4}{\rho^3 v_{\mathrm{R}}^2} \tag{6}$$

where T is the temperature, ρ is the material density and v_{R} is the Rayleigh wave velocity. The proportionality coefficient contains data regarding the bulk phonons and the crystallographic orientation and is considered to be constant for the same material. Note that T is the local temperature at the crack tip and is much higher than the room temperature (Fuller *et al* 1975).

In a developing crack, a surface wave propagates along the crack surfaces. Its emitted EMR frequency is the same as that of the oscillating ions of the crack sides (Rabinovitch *et al* 1998), ω. Therefore, we write $\omega = \omega_{\mathrm{R}}$.

Several important results can be obtained even from these basic ideas.

(a) If the half wavelength, $\lambda/2$, of the atomic perturbation creating the EMR is limited by the crack width 'b' (since at both sides of the crack, atomic movements are restricted), then (Frid *et al* 2000, Rabinovitch *et al* 2000)

$$b \approx \frac{\lambda}{2} = \frac{\pi v_{\mathrm{R}}}{\omega} \tag{7}$$

where v_{R} is the Rayleigh wave velocity. Note that equation (7) reveals that for the same crack width the EMR frequency for stiffer materials would be higher than that for weaker materials. Indeed, since the Rayleigh wave velocity in a material with a given Young's modulus E, Poisson ratio μ and density ρ, is given by

$$v_{\mathrm{R}} = \frac{0.87 + 1.12\mu}{1+\mu}\sqrt{\frac{E}{2\rho(1+\mu)}}$$

the ratio of EMR frequencies for two materials, is given by

$$\frac{\omega_1}{\omega_2} = \frac{(0.87 + 1.12\mu_1)}{(0.87 + 1.12\mu_2)}\frac{(1+\mu_2)}{(1+\mu_1)}\sqrt{\frac{E_1}{E_2}\frac{\rho_2(1+\mu_2)}{\rho_1(1+\mu_1)}}\frac{b_2}{b_1} \tag{7'}$$

To check the validity of equation (7), we compare EMR frequencies and fracture widths for four different materials, the elastic properties of which are shown in table 1.

Table 1. Experimental results of material properties.

	Young's modulus E (GPa)	Poisson ratio μ	Density ρ (kg m^{-3})	Rayleigh wave velocity v_{R} (m s^{-1})
Glass	45	0.2	2600	2448
Glass ceramics	51.6	0.25	2370	2715
Chalk	8.5	0.16	2604	2377
Granite	44.8	0.32	2160	1178

An exact one-to-one correspondence between the EMR signals and the longitudinal splits causing them was obtained only during glass uniaxial compression experiments. Even during the transparent glass–ceramic experiments not all pairs of EMR signal–fracture (S–F) were perfectly related. In our analysis we included only those pairs of S–Fs that could be accurately 'linked'. During chalk and granite (that are non-transparent materials) experiments, a one-to-one link between EMR signals and fractures was not possible. Moreover,

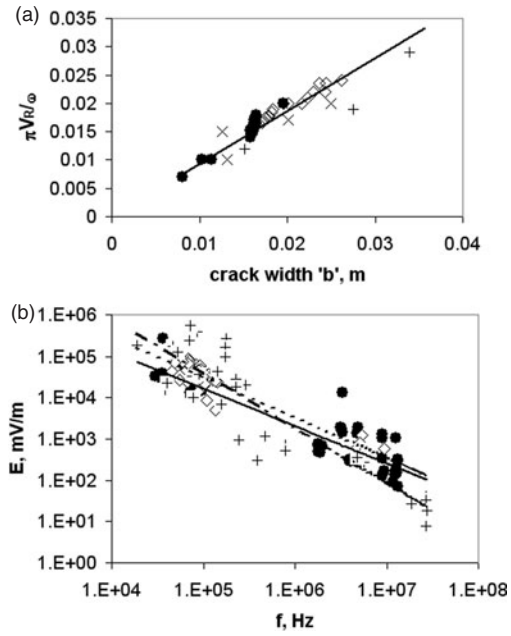

Figure 7. (*a*) The relation between reciprocal EMR frequency and fracture width for chalk, granite, glass and glass ceramics under compression (● chalk, ◊ granite, + glass ceramic, × glass); (*b*) Total compensated field amplitude vs frequency of EMR pulses for chalk, granite and glass ceramic under compression (● chalk, ◊ granite, + glass ceramic; —— chalk trendline, - - - - granite trendline, — · — glass ceramic trendline).

fracture widths and lengths were uncertain since the fracture directions were usually undefined. Hence, we included in our analysis only 'maximal' fractures and, of those, only the ones that had a 'stretched shape', where one dimension (considered as length) was significantly larger than the other (considered to be the fracture width). Figure 7(*a*) shows the plot of '$\pi v_R/\omega$' vs crack width 'b'. The slope of this relation is 0.93 ($R^2 = 0.82$), very close to 1, in agreement with the theoretical prediction (equations (7) and (7′)).

(b) Since EMR pulse amplitude 'A' is proportional to α (equation (4)), which was assumed to be proportional to crack width b, it is expected that the EMR amplitude should be inversely proportional to the EMR signal frequency 'f'.

The voltages of the EMR pulses detected by the antenna depend on antenna reaction (antenna efficiency), which changes with frequency (Rabinovitch *et al* 1999). Compensating for this factor, $E = f(A)$ (E being the field amplitude reaching the antenna), by the appropriate antenna efficiency chart (EHFP-30 Near Field Probe set, Electro-Metrics Penril corporation), we were able to compare the heights of the various EMR signals having different frequencies.

Figure 7(*b*) (Rabinovitch *et al* 1999) shows the compensated amplitudes (E) of the electromagnetic field signals induced by the fracture of chalk, granite and glass ceramic samples.

The analysis of about 160 pulses shows that the amplitude–frequency ratio of each of the three materials can be fitted by a power-law type relation. Thus, for chalk, the relation is $E \cong 6 \times 10^8 f^{-0.91\pm0.04}$ (squared regression coefficient $R^2 = 0.87$), for granite $E \cong 3 \times 10^9 f^{-0.99\pm0.04}$ ($R^2 = 0.89$), and for the glass ceramic $E \cong 2\times10^{11} f^{-1.32\pm0.11}$ ($R^2 = 0.82$). The exponent of these three relationships is close to -1, although for the glass ceramic the value is somewhat shifted. EMR pulses induced by chalk and granite fracture generally showed a single frequency f. In contrast, several EMR pulses associated with glass ceramic fracture were 'multi-frequencied'. Therefore, the amplitude–frequency ratios of these pulses were corrected in the following way. The amplitude at a specific frequency peak of the FFT was calculated by $E(f_i) = E S_i / \sum S_i$, where S_i is the area under the ith peak and E is the measured pulse amplitude. Such a procedure evidently adds errors; it increases the spread of glass ceramic results and could also be the reason for the deviant exponent. Collecting all EMR data on one graph (Rabinovitch *et al* 1999), a single combined relation was obtained: $E \cong 5 \times 10^9 f^{-1.06\pm0.04}$ ($R^2 = 0.84$). These results imply that the amplitude of the EMR field is indeed inversely proportional to the signal frequency and hence is proportional to the crack width.

(c) To check the validity of equation (2) two experimental tests were carried out:

1. Mutual measurement of T' and crack lengths (Bahat *et al* 2002) during transparent glass ceramic failure in compression revealed that T' values varied in the range of 0.8–1.5 μs under low stresses (0.36–1.7 MPa) in association with micro-cracks of several millimetres in length. T' values of 5–15 μs were associated with stresses of up to 65 MPa and were correlated with cracks whose lengths measured several centimetres. A value of T' larger than 20 μs occurred under greater stresses (112 MPa) and was correlated with the longitudinal splitting at failure (∼10 cm).
2. If we assume that the fracture process develops incrementally and that each new increment is proportional to the existing crack length (as previously observed by Gillespie *et al* (1992), and by Cowie and Scholtz (1992a, b), then a log-normal distribution should be expected (Aitchison and Brown 1976). Results show that T' values indeed obey a log-normal distribution (Rabinovitch *et al* 1998).

(d) From (2) and (7),

$$\frac{T'}{\omega} \sim \frac{1}{\pi v_{cr} v_R} S \tag{8}$$

where $S = l \times b$ is the crack area. Since T' and ω are measurable quantities (from the pulse shape, using equation (1)), ratios of crack surface areas, if not their exact values (which need calibration), can be calculated using equation (8). Since crack direction and shape do not change the relation of equation (8), while they are crucial for the separate identification of width and length, T'/ω results are deemed to be more reliable for the correlation with values of crack areas rather than the T' vs length and ω vs width relations distinctly.

Figure 8 shows a representative normalized stress–strain curve of a chalk specimen (out of twenty-four measured samples) together with T'/ω data obtained from EMR measurement during failure (Rabinovitch *et al* 2000). The

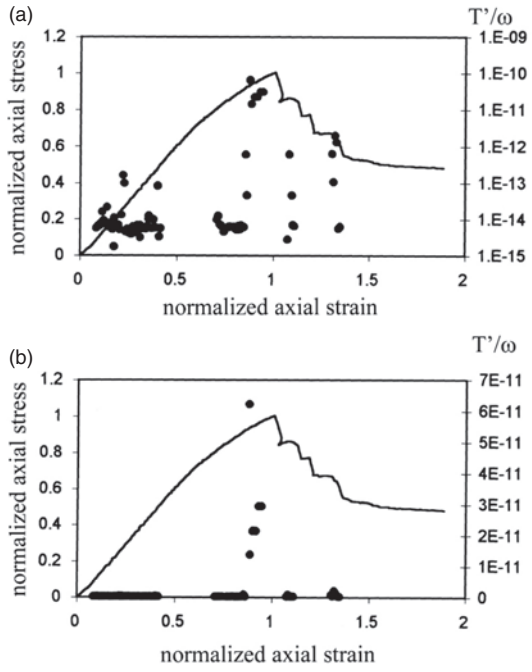

Figure 8. A representative normalized stress–strain curve of a chalk sample together with its T'/ω data: (*a*) the T'/ω data are shown on a semi-logarithmic scale; (*b*) on a normal scale. Stress magnitude and strain are on a normal scale for both (*a*) and (*b*).

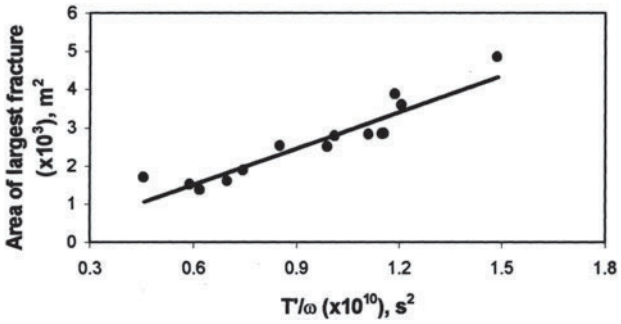

Figure 9. Experimental maximal fracture areas vs largest T'/ω values and a linear fit (squared regression coefficient $R^2 = 0.9$).

values of T'/ω range from 10^{-15} to 10^{-10} (s^2). The minimum values of T'/ω are observed at the beginning of the stress–strain curve. At the elastic and elastic–plastic zones before the peak of the stress–strain curve, T'/ω values of the order of 10^{-14}–10^{-11} s^2 were measured, and the T'/ω value increased to a maximum (of the order of 10^{-10} s^2) in the zone immediately preceding the peak stress. This rapid increase is indicative of the collapse failure. After the peak stress, the T'/ω amplitudes decreased to values of 10^{-14}–10^{-11} s^2 ('relaxation' region).

Fractographic examination of the failed chalk samples revealed fractures ranging in size from 0.1 mm × 0.1 mm up to about 40 mm × 50 mm (Rabinovitch *et al* 2000). This range of crack areas (10^{-2} mm^2 to ∼2000 mm^2) agrees with the same order of magnitude of variation of the T'/ω values. Since a one-to-one correspondence between the EMR pulses and the fractures causing them was not possible in this measurement, only the cracks possessing the largest areas were measured

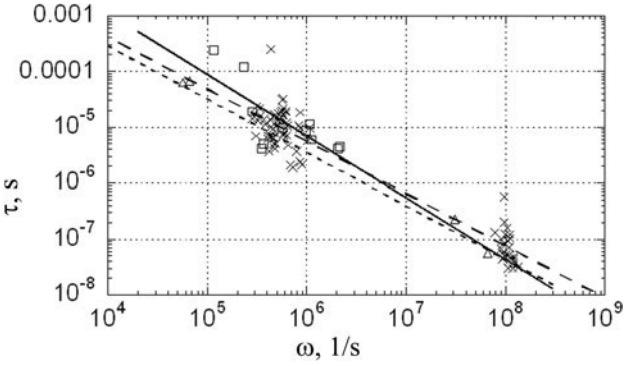

Figure 10. The rise and fall time, τ, as a function of frequency, ω: the points are the experimental results of individual pulses, and the lines are the power law fitting results: for glass (△), fitting $\tau = 1.87\omega^{-0.95}$ (- - - -); for glass ceramics (□), fitting $\tau = 28.1\omega^{-1.1}$ (——); for granite (×), fitting $\tau = 2.23\omega^{-0.93}$ (— — —).

and correlated with the largest T'/ω values (figure 9) (see Bahat *et al* (2001)). As can be seen, very good agreement between equation (8) and the experimental results ($R^2 = 0.9$) was observed.

Hence, these results (the range of values and the correlation of the largest values) support relation (8), and thereby substantiate the validity of the model. Note that no correlation was found between T' and ω or between T' and fracture area (Rabinovitch *et al* 1998). Therefore, it is the relation shown in equation (8) which is directly verified here (figure 9).

(e) To check the validity of equation (6) we compared the τ and ω parameters obtained from analysing EMR pulses induced by fracture in granite, glass and glass ceramics (Rabinovitch *et al* 2003). Figure 10 shows the dependence of τ on ω for glass, glass ceramics and granite. The slopes on a logarithmic scale are -1 ± 0.1 (with $R^2 = 0.96$, 0.85 and 0.91, respectively), agreeing with equation (6). The spread of experimental points in figure 10 can be explained as follows. It has been shown (Fuller *et al* 1975) that the temperature of dynamically propagating cracks rises. The actual rise depends on crack velocity and on material properties (Yatomi 1981). The spread of experimental points can probably be attributed to a spread in crack velocities that causes a spread in temperatures. Note that, by equation (6), $1/\tau \sim T^4$, and hence the dependence on temperature is very strong.

(f) An overall comparison of EMR signals, excited by compression, drilling and blasting shows that their basic shape (equation (1)) is invariant to the dynamic/quasi-static loading mode (Rabinovitch *et al* 2002b). The similarity of shape of single EMR pulses, induced by these three processes, therefore indicates that a unified EMR emitting mechanism is operating behind them all.

4. Survey of the proposed model

4.1. Summary

The suggested model of EMR can be described as follows: following the breaking of bonds, the atoms on both sides of the severed bonds are moved to 'non-equilibrium' positions

relative to their steady state ones and oscillate around them. Lines of oscillating atoms move together and by being connected to atoms around them (in the forward direction and also atoms on their side of the two surfaces newly created by the fracture) the latter also participate in the movement. The ensuing vibrations are similar to those calculated in the Debye model for bulk oscillations. The larger the number of cut bonds, the larger is the area of excited atoms, and hence the greater the EMR amplitude becomes. These oscillations behave like SVOWs, where positive charges move together in a diametrically opposite phase to the negative ones and decay exponentially into the material, like Rayleigh waves. The resulting oscillating electric dipole is the source of the EMR. The pulse amplitude decays by an interaction with bulk phonons.

4.2. Properties of the proposed model

Our model does not suffer from the defects of the earlier ones for the following reasons:

(a) No dislocations are included in the model and, therefore, it can be applied also to brittle and amorphic materials. EMR frequencies obtained experimentally do agree with those of the SVOW.
(b) The spectrum of the SVOW is definitely not of the white noise type. Moreover, it is in line with that given in equation (1) and the measured ones (see, e.g. figure 2(*b*)). In particular, the peak frequency depends on crack width, according to equation (6).
(c) Note that no symmetry breaking mechanism appears in the SVOW model. Furthermore, the crack surface is electrically neutral when time averaged.
(d) (i) Our model is applicable to shear, tensile and even mixed modes of fracture. (ii) The exact correlation between AE and EMR predicted by the 'capacitor' model is not always found experimentally. No such correlation arises in the SVOW model. (iii) Charge neutrality is assured here via a different mechanism ('optical' oscillations). Therefore, no cancellation is expected.

Acknowledgments

This research No 93/02-1 was supported by the Israel Science Foundation, the Earth Sciences Administration of the Ministry of Energy and Infrastructure, and the Izvonot Committee of the Israeli Government Estate Distributions. We are grateful for helpful discussions with R Ben Hador, Y Horowiz and R Thieberger, and for the technical help of V Palchik, M Brima and D Frid. We would like to thank H Hertrich from Solnhofer Bodenplatten-Industrie GmbH and Co KG for help in our experiments.

References

Bahat D 1991 *Tectonofractography* (Heidelberg: Springer)
Bahat D, Rabinovitch A and Frid V 2001 *J. Stuct. Geol.* **23** 1531–47
Bahat D, Frid V, Rabinovitch A and Palchik V 2002 *Int. J. Fracture* **116** 179–94
Cress G O, Brady B T and Rowell G A 1987 *Geophys. Res. Lett.* **14** 331–4
Enomoto Y and Hashimoto H 1990 *Nature* **346** 641–3
Freund F 2000 *Geophys. Res.* **105** 11001–19
Freund F 2002 *J. Geodynamics* **33** 543–70
Finkel V M, Golovin Y I and Sereda V E 1975 *Sov. Phys.—Solid State* **17** 492–5
Frid V 1997 *J. Rock Mech. Rock Eng*. **30** 229–36
Frid V 1998 *J. Appl. Geophys*. **38** 97–104
Frid V, Rabinovitch A and Bahat D 1999 *Phil. Mag. Lett.* **79** 79–86
Frid V 2000 *J. Appl. Geophys.* **43** 5–13
Frid V, Bahat D, Goldbaum J and Rabinovitch A 2000 *Israel J. Earth Sci.* **49** 9–19
Frid V 2001 *Pure Appl. Geophys.* **158** 931–44
Fuller K N G, Fox P G and Field J E 1975 *Proc. R. Soc. Ser.* A **341** 537
Gershenzon N, Zilpimiani D and Manguladze P 1986 *Dokl. Akad. Nauk SSSR* **287** 1–10
Goldbaum J, Frid V, Rabinovitch A and Bahat D 2001 *Int. J. Fract.* 111 L15–20
Hayakawa M *et al* 1993 *Phys. Earth Planet. Inter.* **77** 127–35
Jagasivamani V and Iyer K J L 1988 *Mater. Lett.* **6** 418–22
Khatiashvili N 1984 *Izv. Earth Phys.* **20** 656–61
King C Y 1983 *Nature* **301** 377
King P J and Sheard F W 1970 *Proc. R. Soc. Ser.* A **320** 175
Kittel C 1987 *Quantum Theory of Solids* (New York: Wiley)
Langford S C and Dickinson J T 1987 *ACS/Symp. Ser.* **415** 224–46
Miroshnichencko M and Kuksenko V 1980 *Sov. Phys.—Solid State* **22** 1531–3
Misra A A 1977 *Appl. Phys.* **16** 195–9
Misra A and Ghosh S 1980 *Appl. Phys.* **23** 387–90
Molotskii M I 1980 *Sov. Tekh. Phys. Lett.* **6** 22–3
Nitsan U 1977 *Geophys. Res. Lett.* **4** 333–6
O'Keefe S G and Thiel D V 1995 *Phys. Earth and Planet. Inter.* **89** 127–35
Ogawa T, Oike K and Miura T 1985 *J. Geophys. Res.* **90** 6245–49
Petrenko V F 1993 *Phil. Mag.* B **67** 301–15
Rabinovitch A, Bahat D and Frid V 1995 *Int. J. Fract.* **71** r33–41
Rabinovitch A, Bahat D and Frid V 1996 *Z. Geol. Wiss.* **24** 361–8
Rabinovitch A, Frid V and Bahat D 1998 *Phil. Mag. Lett*. **5** 289–93
Rabinovitch A, Frid V and Bahat D 1999 *Phil. Mag. Lett.* **79** 195–200
Rabinovitch A, Frid V, Bahat D and Goldbaum J 2000 *Int. J. Rock Mech. Mining Sci.* **37** 1149–54
Rabinovitch A, Bahat D and Frid V 2002a *Int. J. Rock Mech. Mining Sci.* **39** 125–9
Rabinovitch A, Frid V and Bahat D 2002b *Phys. Rev.* E **65** 011401-4
Rabinovitch A, Frid V, Bahat D and Goldbaum J 2003 *J. Appl. Phys.* **93** 5085–90
Sakai H, Oda H, Nakayama T and Doi H 1992 *J. Phys. Earth* **40** 447–58
Schiff L I 1986 *Quantum Mechanics* 3rd edn (London: McGraw-Hill)
Srivastava G P 1990 *The Physics of Phonons* (Bristol: Adam Hilger)
Tetelman A S and McEvly A J 1967 *Fracture of Structural Materials* (New York: Willey)
Tomizawa I *et al* 1994 *Electromagnetic Phenomena Related to Earthquake Prediction* (Tokyo: Terra Scientific) pp 337–47
Tomizawa I and Yamada I 1995 *J. Geomagn. Geoelect.* **47** 313–24
Ueda S and Al-Damegh K S 1999 *Evaluation of VAN Method. Atmospheric and Ionospheric Electromagnetic Phenomena Associated with Earthquakes* (Tokyo: Terra Scientific)
Urusovskaja A A 1969 *Sov. Phys.—Usp.* **11** 631–43
Vozoff and Frid 2001 *Symp. on Geological Hazards (Rafferety's Resort Newcastle, 15–16 November 2001)*
Warwick J W, Stoker C and Meyer T R 1982 *J. Geophys. Res.* B **87** 2851–9
Yamada I, Masuda K and Mizutani H 1989 *Phys. Earth Planet. Int.* **57** 157–68
Yatomi C 1981 *Eng. Fract. Mech.* **14** 759
Yoshida S 2001 *J. Geophys. Res.* **106** 2103–20